SCIENTIFIC REPᴏRTS

OPEN

High-performance MnO$_2$-deposited graphene/activated carbon film electrodes for flexible solid-state supercapacitor

Lanshu Xu, Mengying Jia, Yue Li, Xiaojuan Jin & Fan Zhang

High theoretical capacitance of MnO$_2$ nanoparticles were successfully electrodeposited on the conductive graphene/activated carbon (GN/AC) composite film, and the urchin type MnO$_2$ microspheres were controlled by adjusting the electro-deposition reaction times. The GN/AC/MnO$_2$-1200s composite electrodes exhibited a maximum specific capacitance of 1231 mF/cm^2 (MnO$_2$ loading mass of 7.65 mg/ cm^2 and the mass specific capacitance of 123 F/g) at a current density of 0.5 mA/cm^2. The assembled flexible solid-state symmetric supercapacitor had a good mechanical flexibility (about 88.6% of its original capacitance after 500 bending times) and prominent cycling stability (about 82.8% retention in capacitance over 10000 cycles). More importantly, the device could possess a maximum energy density of 0.27 mWh/cm^3 and a maximum power density of 0.02 W/cm^3. These results well demonstrate a great potential for applications of GN/AC/MnO$_2$ composite electrodes in flexible energy storage devices.

Graphene (GN), an atom-thick, honeycomb two-dimensional structure, has the characteristics of higher specific surface area, excellent conductivity or mechanical flexibility[1–3]. It has attracted a great deal of concerns and is widely used in flexible composite electrodes[4–7]. However, the preparation process of graphene is extremely complex, high-cost and especially prone to agglomeration or stacking, which seriously affect the infiltration of the electrolyte and reduce the utilization ratio of specific surface area[8]. Activated Carbon (AC), as the earliest and the most widely application of electrode materials in supercapacitors (SCs), possesses the advantages of larger specific surface area, higher electrochemical stability, low price, environmental friendliness, rich raw materials and renewable, etc[9–11]. The composition of GN/AC can be applied in the field of flexible electrodes and achieve a significant synergistic effect. The two-dimensional flake GNs serve as adhesive to bond ACs together by self-assembly method, which made the composite electrodes have good mechanical flexibility and provide a conductive bridge for ion transport. Meanwhile, the doping of AC expands the layer spacing and can prevent the agglomeration or stacking of GN in some extent. Moreover, the formed three-dimensional (3D) porous structure also can increase the specific surface area and improve the electrical conductivity. AC is a promising partial substitute for GN in flexible electrodes.

Manganese oxide materials are widely known as the pseudocapacitance based on reversible redox reactions at the surface of active materials[9,12]. Compared with other metal oxides, MnO$_2$ electrodes have significant advantages of low price, high theoretical specific capacitance and environmental compatibility[13–15]. However, there are still significant drawbacks of MnO$_2$ electrodes. Namely, the low electronic conductivity leads to relative low power density, and the low cycling life due to the disproportionate dissolution reaction of MnO$_2$ active material, which results in fast performance fading during cycling[16–18]. The key to solve these problems is to explore a novel flexible electrode material system containing the material combination, material morphology and distribution, and choice of electrolytes that even under high voltages, high electrical conductivity and electrochemical stability can be guaranteed[19,20]. In recent years, researches have explored many possible routes using different flexible electrode materials, such as carbon nanotubes (CNTs)[21], reduced graphene oxide (rGO)[22], rGO/CNTs[23], MnO$_2$/ rGO[24] and so on. For example, CNT supercapacitor showed an energy density of 0.601 mWh/cm^3 and rGO supercapacitor displayed a value of 0.17 μWh/cm^3. The energy density could be generally increased by well designing
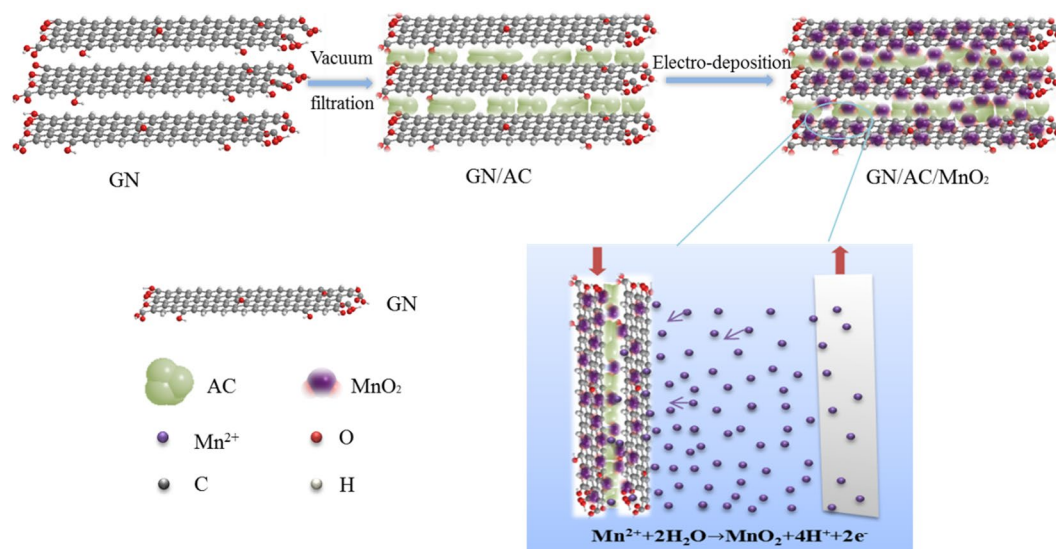
Figure 1. Schematic illustrations for the preparation process of GN/AC/MnO2 composite electrodes.

the composite structures. An emerged strategy of combining renewable carbon-based materials with pseudoca-pacitive MnO_2 can achieve cost and environmental advantages, high electrochemical performance, and long cycle life, benefiting from both mechanisms of double-layer supercapacitor and pseudocapacitor[25–28].

In this work, a flexible and binder-free ternary $GN/AC/MnO_2$ composite electrode film was successfully syn-thesized by facile vacuum filtration and electro-deposition processes. The porous AC materials were interspersed between GN sheets as electrode substrates, facilitating the electrolyte ion transport and the deposition of MnO_2. The effects of MnO_2 morphology on the GN/AC composite films were controlled by simply adjusting the reaction times and the possible deposition mechanism of MnO_2 was derived. Moreover, the electrochemical performances and mechanical property were systematically studied. As expected, the measurement results indicated that the MnO_2 morphology greatly affected the electrochemical performance of $GN/AC/MnO_2$ composite electrodes, and the flexible ternary electrode exhibited a high specific capacitance of 1231 mF/cm² at a current density of 0.5 mA/cm². Furthermore, the as-assembled flexible solid-state SCs showed a stable electrochemical performance and higher energy density.

Results

$GN/AC/MnO_2$ composite electrodes were prepared by two steps (Fig. 1): firstly, AC particles were bonded together with two-dimensional GN sheets using self-assembly method by a facile vacuum filtration process, which expanded the layer spacing and increased the specific surface area of GN. Secondly, the resulted GN/AC flexible films were used as the working electrode and MnO_2 nanostructures were electrodeposited on the surface of GN/AC flexible films. The formation mechanism can be summarized briefly. GN/AC flexible films were immersed into a plating solution containing $Mn(CH_3COO)_2$ and Na_2SO_4. In anodic constant current electro-deposition process, the charged ions in the electrolyte were directed diffusion under an applied electric field, low valence metal ions were discharged near the anode and the high valence ions were formed, leading to Mn (II) was oxidized into Mn (IV). The redox reaction occurred on the electrode surface: $Mn^{2+} + 2H_2O \rightarrow MnO_2 + 4H^+ + 2e^-$.

Figure 2a showed the TEM image of GN sheets. The layered graphene tended to stack together to form agglomerate due to the chemical inertness of reduced graphene oxide[29]. From that we can see the obtained GN was very well dispersed as a single-layer sheet. The porous ACs can be seen in Fig. 2b, the highly porous mor-phology was beneficial to the transmission of electrolyte ions. The SEM images (Fig. 2c) of the GN/AC flexible film showed that the GN sheets resembled adhesive to connect ACs together and provided a conductive bridge for ion transport. Obviously, the porous carbon materials and the formed wavy surface increased the specific surface area of GN. Also can be seen from the cross-section image (insert in Fig. 2c), the AC particles were inter-spersed in GN layers, which extended the interlayer spacing and prevented the flocculation and accumulation of GN sheets to some certain extent. The extended GN/AC flexible film was conducive to the deposition of MnO_2. Figure 2d–h showed the growth of MnO_2 microspheres on GN/AC flexible films in the electro-deposition process with various reaction times of 300 s, 600 s, 900 s, 1200 s and 1500 s. As shown in Fig. 2d, small MnO_2 nanoparticles were deposited on the film surface when the reaction time was 300 s. A dense MnO_2 nanoparticle layers were formed on the GN/AC flexible films with the reaction time increased to 600 s (Fig. 2e). The uniform structure of GN/AC films with strong adhesion and good mechanical property could provide a large surface area, there-fore, a higher number of active sites, leading to extensive coverage of MnO_2 nanoparticles. Further increasing the reaction time from 600 s to 1200 s, the morphology and structure of $GN/AC/MnO_2$ composite films were significantly changed. A large quantity of MnO_2 microspheres were gradually formed and observed on the sur-face (Fig. 2f,g). The electric potential continued to increase with further increase of reaction time at the current density of 8 mA/cm². The higher electric potential might be conducive to nucleation and negatively inhibit crystal growth. When the deposition time reached 1500 s (Fig. 2h), more MnO_2 microspheres generated and stacked
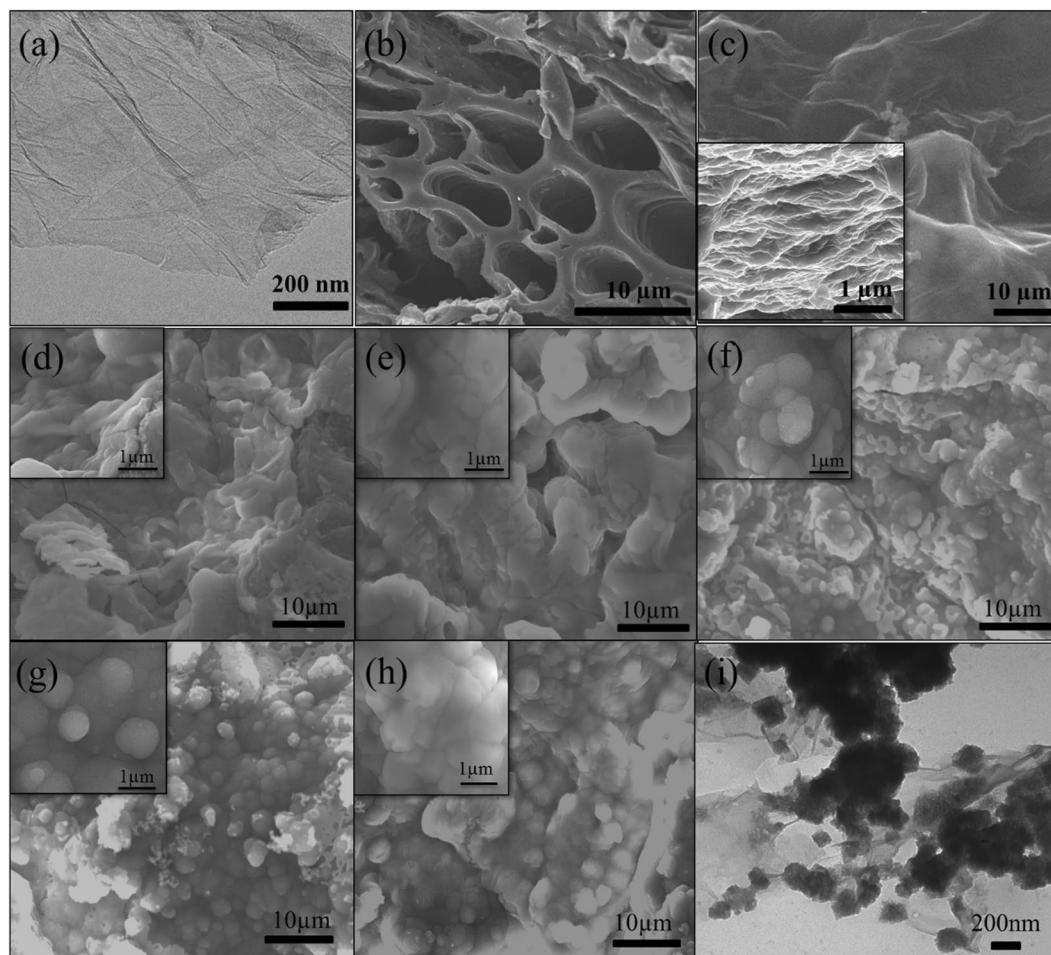
Figure 2. (**a**) TEM image of GN sheet; (**b**) FESEM image of ACs; (**c**) SEM image of flexible GN/AC substrate; SEM images of GN/AC/MnO2 composite films prepared at various reaction times: (**d**) 300 s, (**e**) 600s, (**f**) 900s, (**g**) 1200s and (**h**) 1500s; (**i**) TEM image of GN/AC/MnO2-1200s composite films.
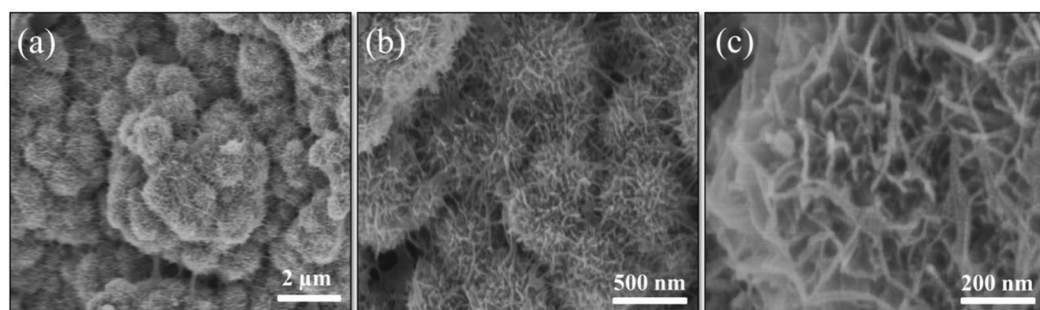
**Figure 3.** GN/AC/MnO2-1200s composite films at high magnification.

together, the accumulation of MnO_2 nanoparticles layer might cause the film too dense (~8.25 mg/cm^2 mass loading), which decreased the specific surface area and was not conducive to ion transport. The TEM image of GN/AC/MnO$_2$-1200s was showed in Fig. 2i, it can be observed that MnO_2 microspheres were uniformly dispersed in flexible substrate. In addition, the AC/MnO$_2$ attached to the surface of GN forming a distinct obstacle between GN layers, increasing the specific surface area, which is beneficial to improve the electrochemical properties. Moreover, high-magnification FESEM images of GN/AC/MnO$_2$-1200s were displayed in Fig. 3a,b and c. The formed MnO_2 microspheres, similar to urchins, have a diameter of 150–300 nm. Obviously, the formation of urchin type MnO_2 microspheres dramatically increased the specific surface area of the active materials, which benefited to the infiltration and transmission of the electrolyte. Moreover, the urchin type MnO_2 microspheres can be easily controlled by simply adjusting the electro-deposition reaction times.
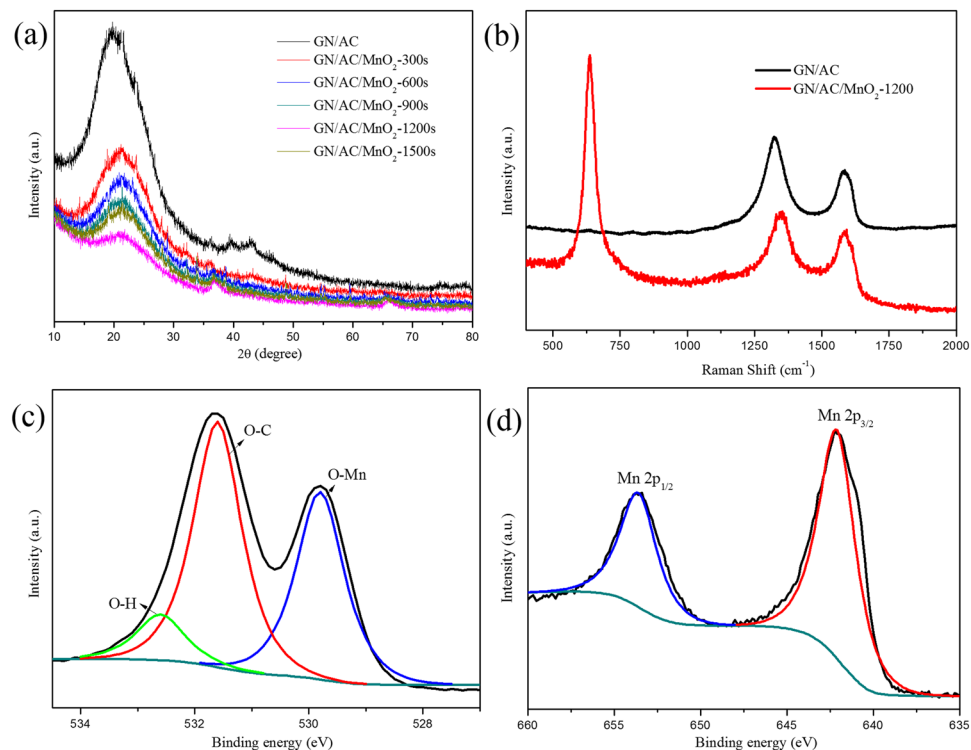
**Figure 4.** (**a**) XRD patterns, (**b**) Raman spectra, XPS spectra (**c**) O 1s, (**d**) Mn 2p.

The X-ray diffraction (XRD) for GN/AC and GN/AC/MnO$_2$-1200s were further analyzed. As shown in Fig. 4a, two diffraction peaks (2Θ) was observed at around 22° and 43° for the GN/AC composites, corresponding to the (002) and (101) crystal planes, respectively, which are the characteristic peaks of carbon-based material[30,31]. With the increase of MnO$_2$ deposition, the intensity of carbon-based characteristic peaks decreased accordingly, especially for GN/AC/MnO$_2$-1200s composite film. Moreover, two sharp peaks around 37° and 66° appeared for GN/AC/MnO$_2$ composite films, which could be indexed to the birnessite-type MnO$_2$ (JCPDS 42-1317)[32,33]. To further elucidate the detailed structures and chemical compositions of MnO$_2$ microspheres on GN/AC (1200 s) films, Raman spectra and X-ray photoelectron spectroscopy (XPS) were probed, and the results were shown in Fig. 4b and Fig. 4c,d. As presented in Fig. 4b, the GN/AC flexible films exhibited two obvious peaks around 1320 cm^{-1} and 1580 cm^{-1}, corresponding to the D band and G band of carbon-based material, respectively. After the deposition of MnO$_2$ on GN/AC film for 1200 s, a sharp peak around 635 cm^{-1} appeared, which could be assigned to the (O-Mn) stretching vibration of divalent Mn ions, and the broad peak might be ascribed to the overlap of various characteristic peaks from MnO$_2$, Mn$_3$O$_4$ and MnOOH[9,34]. Moreover, the I$_D$/I$_G$ ratio of GN/AC films increased to 1.22 from 1.21 after electro-deposited MnO$_2$, indicating that the deposition of MnO$_2$ on GN/AC films had a slight increase of defect ratio and a negligible effect on the structure of the substrate. Typical XPS spectra of O 1 s and Mn 2p for MnO$_2$ electro-deposited GN/AC at 1200 s were shown in Fig. 4c,d. From the Fig. 4c, we can see that three peaks at around 529.8, 531.6 and 532.6 eV in the O 1 s spectra, which corresponded to the O-Mn, O-C, and O-H bonds, respectively[35]. The high-resolution Mn 2p spectra was presented in Fig. 4d, from which can be seen that two binding energies were centered at 642.1 eV and 653.7 eV, corresponding to Mn 2p$_{3/2}$ and 2p$_{1/2}$ peak, respectively, with a spin energy separation of 11.6 eV, which revealed a mean valence state of 4+ for Mn in MnO$_2$ and matched well with previously reported[36,37]. Furthermore, the result was consistent with XRD analysis as mentioned above.

The electrochemical performances of the GN/AC/MnO$_2$ composite electrodes were firstly evaluated by CV and GCD curves using a three-electrode system in 1.0 M Na$_2$SO$_4$ aqueous electrolyte. Figure 5a compared the CV curves of the GN/AC/MnO$_2$ composite electrodes with various MnO$_2$ deposition times ranging from 0 to 1500 s in a potential window of 0–1.0 V at the same scan rate of 10 mV/s. The ternary composites of GN/AC/MnO$_2$ have a larger enclosed area than binary composite of GN/AC, indicating that MnO$_2$-deposited on the GN/AC flexible films greatly enhanced the electrochemical performance due to the synergistic effects. The addition of ACs expanded the layer spacing of GN sheets, facilitating the deposition of MnO$_2$, which was beneficial to enhance the electrochemical properties. The specific capacitance can be calculated from CV curves based on Equation (1) and plotted in Fig. 5b. The area specific capacitances of GN/AC/MnO$_2$-1200s electrodes (520 mF/cm^2 at a scan rate of 10 mV/s) were much larger than others, and then it decreased slightly when the deposition time increased to 1500 s. Moreover, as the amount of MnO$_2$ deposition increases, the mass specific capacitances of the composite electrodes are going to decrease accordingly. But for applications such as flexible and small energy storage devices, the amount of energy stored per area is more important than energy per mass[38]. Figure 5c showed GCD curves of all samples at a current density of 1 mA/cm^2. The triangular shapes were slightly deformed, indicating that the
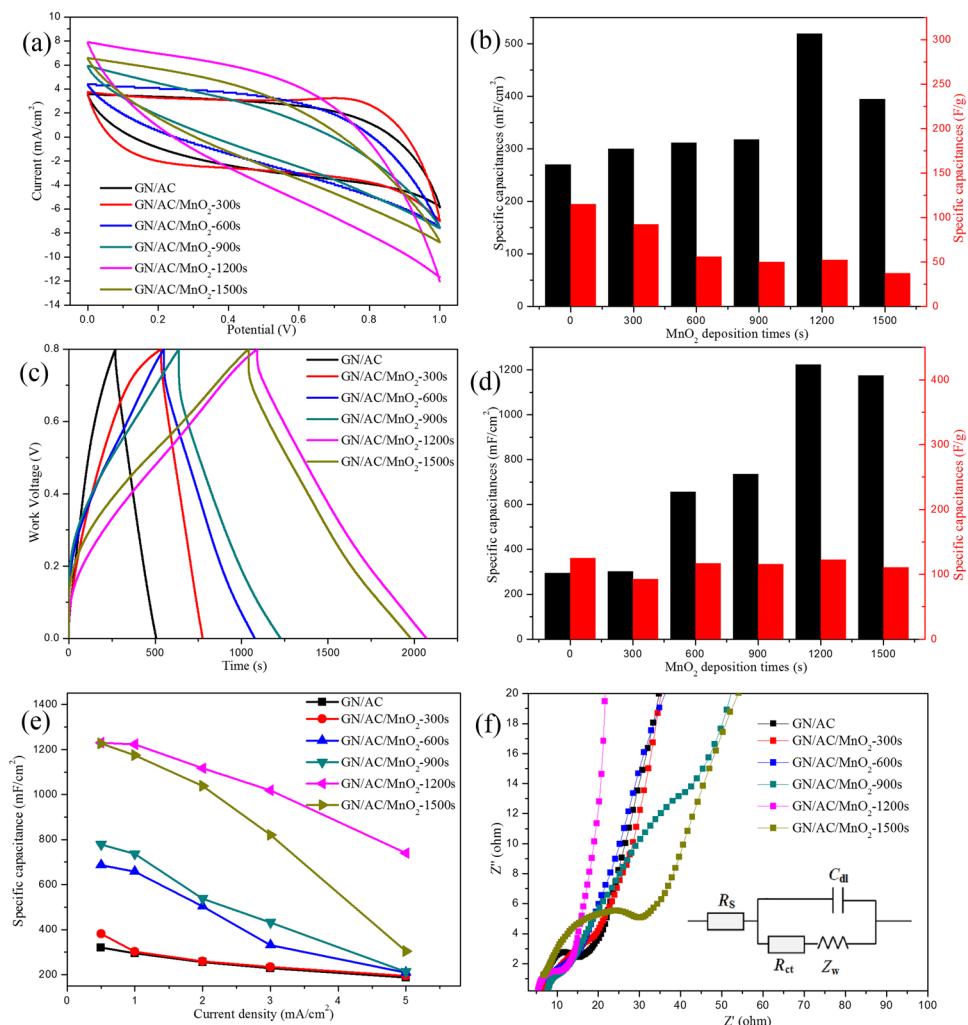
Figure 5. (**a**) CV curves of all samples at the scan rate of 10 mV/s; (**b**) Specific capacitances of all samples at 10 mV/s under the different deposition times; (**c**) GCD curves of all samples at the current density of 1 mA/cm2; (**d**) Specific capacitances of all samples at 1 mA/cm2 under the different deposition times; (**e**) Specific capacitances of all samples at various current densities; (**f**) Nyquist plot of all samples.

capacitance came from the combination of both electrochemical double-layer capacitance and pseudocapacitance[39]. Similar to the CV curves, the GN/AC/MnO$_2$-1200s possessed the longest discharge time than others. According to the Equation (2), the specific capacitances with different deposition times were calculated and plotted in Fig. 5d. For the GN/AC, GN/AC/MnO$_2$-300, 600, 900, 1200 and 1500 s composite electrodes, the corresponding specific capacitances were 295 (125), 302 (93), 658 (117), 736 (116), 1224 (122), 1175 mF/cm^2 (111 F/g), respectively. It should be noted that GN/AC/MnO$_2$-1200s has a higher specific capacitance of 1224 mF/cm^2 at 1 mA/cm^2, and the mass specific capacitance was around 122 F/g with a mass of 0.01 g/cm^2 (MnO$_2$ loading mass of 7.65 mg/cm^2). Moreover, It is worth pointing out that such mass loading of MnO$_2$ is much higher than other reported literatures[40], indicating a much larger surface area of GN/AC flexible films[41]. Based on the above electrochemical measurements, the results could be proved that the optimized electro-deposition time was 1200 s for GN/AC/MnO$_2$ electrodes. Furthermore, the area specific capacitances of all samples calculated by GCD curves were showed in Fig. 5e. Obviously, GN/AC/MnO$_2$-1200s composite electrodes had a dramatic specific capacitance of 1231 mF/cm^2 (mass specific capacitance of 123 F/g) at 0.5 mA/cm^2, more than 3.85 times higher than GN/AC flexible films (320 mF/cm^2). Upon increasing the current density up to 5 mA/cm^2, the specific capacitance of GN/AC/MnO$_2$-1200s composite electrodes (740 mF/cm^2) could retain about 60% of its original values, and more than 3.98 times higher than GN/AC flexible films (186 mF/cm^2). For GN/AC/MnO$_2$-1500s, the specific capacitance decreased prominently from 1227 mF/cm^2 at 0.5 mA/cm^2 to 304 mF/cm^2 at 5 mA/cm^2, which only retained about 25%. The decrease of the specific capacitance was ascribed to the excessive deposition time, which might cause the film too compact and deteriorate the ion transport. Further demonstration can be seen in Fig. 5f, the GN/AC/MnO$_2$-1500s electrode had a large resistivity (R_s, ~21.11 Ω), which was not benefit for electron transport. The Nyquist plot of GN/AC/MnO$_2$-1200s composite started from the Z'-axis and progressed almost vertically to the Z''-axis at the low frequency, indicating that the ideal capacitive characteristics of the electrode[42].
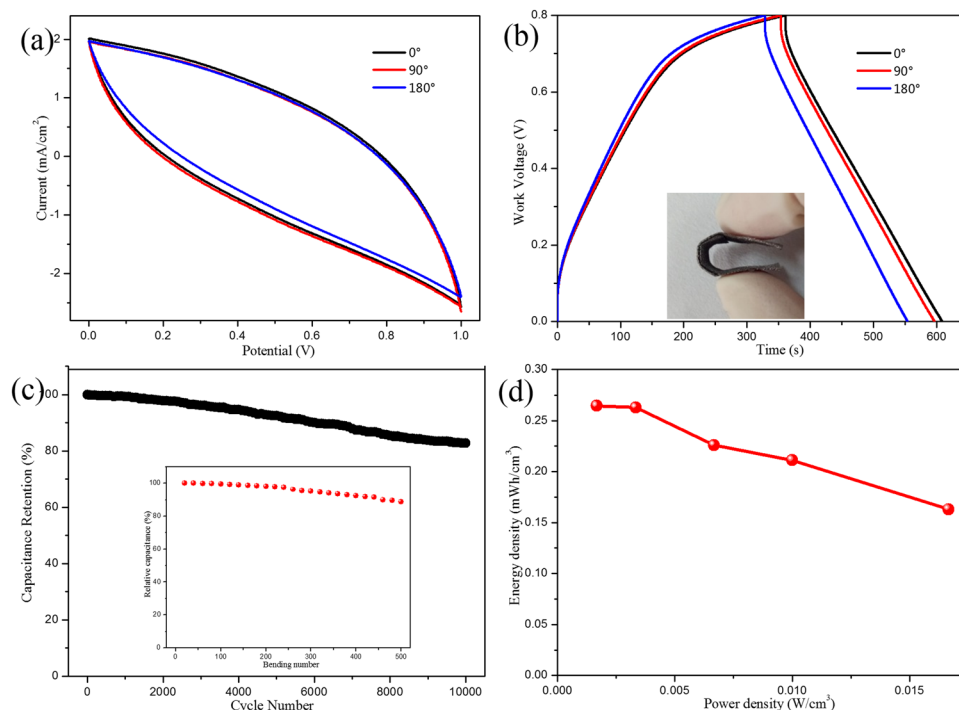
Figure 6. (**a**) CV curves of the flexible devices at 10 mV/s under different bending angles; (**b**) GCD curves of the flexible devices at 1 mA/cm2 under different bending angles; (**c**) Cycling stability of the flexible devices over 10000 cycles and the inset is the mechanical flexibility under different bending times; (**d**) Energy density as a function of power density.

To explore the superior performances of 3D GN/AC/MnO$_2$ electrodes in flexible energy storage devices, symmetric flexible solid-state SCs have been assembled by fixing two GN/AC/MnO$_2$-1200s electrodes in parallel with PVA/Na$_2$SO$_4$ electrolyte. As can be seen from Fig. 6a and b, CV curves and GCD curves were nearly overlapped when the bending angles of the flexible device varied from 0° to 180°. And only about 10% fading for the specific capacitance when bended to 180°, demonstrating the electrodes had negligible influence on folding or bending. Using Equation (3), the volumetric capacitance of flexible GN/AC/MnO$_2$ device was 2.96 F/cm^3 at 1 mA/cm^2. Evidently, the volumetric capacitance is considerably superior to recently reported devices, such as H-TiO$_2$@MnO$_2$//H-TiO$_2$@C (0.70 F/cm^3 at 0.5 mA/cm^2)[37], RGO//MnO$_2$ (0.75 F/cm^3 at 10 mV/s)[40], MnO$_2$//Fe$_2$O$_3$ (1.5 F/cm^3 at 2 mA/cm^2)[43], MnO$_2$//Fe$_2$O$_3$ (1.2 F/cm^3 at 10 mV/s)[44], MnO$_2$//Ti-Fe$_2$O$_3$@PEDOT (2.40 F/cm^3 at 1 mA/cm^2)[45]. For practical application, the cycling stability and mechanical flexibility were conducted. As shown in Fig. 6c, approximately 82.8% retention in capacitance over 10000 cycles and the capacitance still maintained at 88.6% of its original value after 500 bending times at 5 mA/cm^2, indicating the device had an excellent stability and good mechanical flexibility. Furthermore, according to Equations (4) and (5), the calculated energy densities E and power densities P of our flexible SCs are shown in Fig. 6d. The as-assembled device can possess a maximum energy density of 0.27 mWh/cm^3 at 0.5 mA/cm^2 and a maximum power density of 0.02 W/cm^3 at 5 mA/cm^2. Therefore, we can determine that the flexible GN/AC/MnO$_2$ SCs, with a good mechanical flexibility and superior electrochemical performance, are promising candidates for assembling flexible, environment friendly, low price and ultrathin SCs.

Discussion

In summary, we reported a two-step process for constructing a 3D GN/AC/MnO$_2$ flexible electrode using vacuum filtration and electro-deposition methods. The synergistic effects among 2D graphene sheets, porous activated carbon and high theoretical capacitance of MnO$_2$ conduced to obtain excellent electrochemical performance. The 3D GN/AC substrate facilitated the growth of MnO$_2$ and enhanced the conductivity. The urchin type MnO$_2$ microspheres could be simply controlled by adjusting the electro-deposition reaction times. The GN/AC/MnO$_2$-1200s composite electrodes exhibited a maximum specific capacitance of 1231 mF/cm^2 with a mass of 0.01 g/cm^2 (MnO$_2$ loading mass of 7.65 mg/cm^2) at a current density of 0.5 mA/cm^2. Furthermore, approximately 82.8% retention in capacitance over 10000 cycles and the capacitance still maintained at 88.6% of its original value after 500 bending times. In addition, the as-assembled device could possess a maximum energy density of 0.27 mFmWh/cm^3 at 0.5 mA/cm^2 and a maximum power density of 0.02 W/cm^3 at 5 mA/cm^2. These results well prove that our GN/AC/MnO$_2$ composite electrodes have broad prospects in flexible and wearable electronic products.

Experimental

Chemicals and materials. Graphite powers were purchased from Alfa Aesar and waste fiberboard materials were used to product ACs. Sodium nitrate (NaNO$_3$), sulfuric acid (H$_2$SO$_4$), potassium permanganate (KMnO$_4$), hydrochloric acid (HCl), manganese(II) acetate tetrahydrate [Mn(CH$_3$COO)$_2$·4H$_2$O] and sodium sulfate

(Na_2SO_4) were obtained from Sinopharm Chemical Reagent Co., Ltd (Beijing, China). All chemicals were used as received without further purification.

Preparation of graphene oxide sheets.
Ultrathin graphene oxide (GO) sheets were obtained by chemical treatment of exfoliated graphite powders according to the modified Hummers' method[46,47]. Typically, 3 g of graphite powers and 1.5 g of $NaNO_3$ were added into 70 mL of 98% H_2SO_4 and stirred in an ice-water bath. Subsequently, 9 g of $KMnO_4$ was added slowly. After 2 h, the obtained mixture was transferred into the water bath and kept at 35 °C for 30 min. Next, 150 mL of deionized water was added gradually, meanwhile, the temperature was maintained lower than 50 °C by controlling the speed of dripping water. After that, the water bath was raised up to 95 °C and kept constant for 30 min. Then, 15 mL of 30% H_2O_2 solution and 50 mL of warm deionized water were dropped into the mixture to obtain the diluted bright yellow suspension. The resulting suspension was cleaned using HCl aqueous (1:10) solution and deionized water. Finally, the obtained GO solution was carefully diluted into 2 mg/mL using deionized water.

Preparation of porous AC materials.
Waste fiberboard materials were supplied by Beijing Jiahekailai Furniture and Design Company, which contained 12wt % urea-formaldehyde resin adhesive. Firstly, the materials were carbonized in a high-purity nitrogen atmosphere and heated to the temperature of 500 °C at the heating rate of 10 °C/min, then maintained for 60 min. After carbonization, the obtained materials were mixed with KOH at the mass ratio of 1:3 and further activated at the temperature of 750 °C for 60 min in oven. Finally, the activated ACs were washed and filtered using deionized water and 1 M HCl solution respectively until to neutral pH. Then dried at 105 °C for 8 h and stored for subsequent use[48,49].

Preparation of GN/AC flexible films.
The AC powder and acetylene black with a mass ratio of 9:1 were mixed and dispersed in N,N-dimethylformamide (DMF) under ultrasonic vibration to produce a homogeneous dispersion of 0.5 mg/mL. Based on the premise of ensuring the formation of flexible film, AC was used to replace GN with the maximum limit. 5 mL of GO suspension was mixed with 40 mL of AC dispersion, corresponding 5 mL of DMF was added in Erlenmeyer flask to ensure that the volume ratio of water to DMF was 1:9, which was advantageous to improve the dispersion of GO[50]. Then the mixture solution was sealed with preservative film and under ultrasonic vibration for 2 h. Subsequently, a small quantity of 80% hydrazine hydrate was added in the resulting homogeneous dispersion. The weight ratio of hydrazine hydrate to GO was about 7:10[51]. After being vigorously shaken or stirred for 5 min, the Erlenmeyer flask was put in a water bath (~95 °C) for 3 h. Finally, the mixture solution was vacuum-filtrated on the organic microporous membrane filter at constant pressure.

Preparation of GN/AC/MnO$_2$ composite electrodes.
In order to prepare the GN/AC/MnO_2 composite electrodes, the three-dimensional GN/AC flexible films were cut into 1×1.5 cm pieces and an electro-deposition process was performed in a three-electrode system with GN/AC substrate as the working electrode, platinum plate electrode as counter electrode, and calomel electrode as reference electrode. The electrolyte contained 0.5 M $Mn(CH_3COO)_2 \cdot 4H_2O$ and 0.5 M Na_2SO_4. Anodic constant current deposition method (at the current density of 8 mA/cm^2) was applied to deposit MnO_2 on the working electrode. The GN/AC/MnO_2 composite electrodes at different reaction times were donated as GN/AC/MnO_2-x, where x is the reaction time (s). The weight of MnO_2 in GN/AC/MnO_2 electrode was calculated by weighing before and after the GN/AC loading MnO_2 (Mettler ToledoXP56, resolution of 1 μg).

Assembly of flexible solid-state SCs.
Two pieces of the flexible electrode films of GN/AC/MnO_2 were immersed in the hot Na_2SO_4/Polyvinyl alcohol (PVA) gel electrolyte (3 g Na_2SO_4 and 3 g PVA were added into 30 mL deionized water) for 60 min, and subsequently picked out for air-drying to evaporate the residual water. Then, they were assembled in parallel and packaged together by Ni foam. Finally, the device was pressed under a pressure of ~1 MPa for 30 min, which can make them adhere tightly and facilitate the polymer gel electrolyte penetrating into them.

Characterizations.
The microscopic morphologies of the composites were characterized by scanning electron microscopy (SEM, JEOL JSM-7001F), transmission electron microscopy (TEM, JEM-1010) and field emission scanning electron microscopy (FESEM, SU8010). X-ray diffraction (XRD) was used to analyze the crystal structure of the composites using a Bruker D8 diffractometer with Cu Kα radiation. Raman spectra were collected by a LabRAM HR Evolution Raman spectroscope using a 532 nm laser source. X-ray photoelectron spectroscopy (XPS) characterizations were conducted using an Axis Ultra DLD X-ray photoelectron spectroscopy.

Electrochemical measurements.
Electrochemical performances of the composites were evaluated by a CHI 660D electrochemical workstation using a three-electrode system, in which platinum plate electrode and saturated calomel electrode were used as counter electrode and reference electrode in an 1 M Na_2SO_4 aqueous solution, respectively. The GN/AC/MnO_2 composite electrode was used as the working electrode. Cyclic voltammetry (CV), galvanostatic charge/discharge (GCD), impedance spectroscopy (EIS) and cycling stability were measured systematically. The areal or volumetric specific capacitance ($C_{s,electrode}$ or $C_{V,cell}$) of single electrode or flexible SCs were calculated by the CV and GCD curves using the following equations:

$$C_{s,electrode} = \frac{1}{S_{electrode} v \Delta V} \int I(V) dV$$

(1)

$$C_{s,electrode} = \frac{I\Delta t}{S_{electrode}\Delta V} \qquad (2)$$

$$C_{V,cell} = \frac{I\Delta t}{V_{cell}\Delta V} \qquad (3)$$

The energy density (E_V, mWh/cm³) and power density (P_V, W/cm³) was calculated by the following equations:

$$E_V = \frac{1}{2}C_{V,cell}\Delta V^2 \qquad (4)$$

$$P_V = \frac{E_V}{\Delta t} \qquad (5)$$

where I (A) is the charge/discharge current, v (mV/s) is the scan rate, Δt (s) is the discharging time, $S_{electrode}$ (cm²) is the area of single electrode, V_{cell} (cm³) is the volume of flexible SCs, and ΔV is the potential window.

References

1. Wang, X. & Shi, G. Flexible graphene devices related to energy conversion and storage. *Energy & Environmental Science* **8**, 790–823 (2015).
2. Xu, Y. *et al.* Flexible solid-state supercapacitors based on three-dimensional graphene hydrogel films. *Acs Nano* **7**, 4042–4049 (2013).
3. Tian, H. *et al.* Flexible electrostatic nanogenerator using graphene oxide film. *Nanoscale* **5**, 8951–8957 (2013).
4. Clerici, F. *et al.* In situ MoS₂ Decoration of Laser-Induced Graphene as Flexible Supercapacitor Electrodes. *Acs Applied Materials & Interfaces* **8**, 10459–10465 (2016).
5. Guo, M. X., Bian, S. W., Shao, F., Liu, S. & Peng, Y. H. Hydrothermal synthesis and electrochemical performance of MnO₂/graphene/polyester composite electrode materials for flexible supercapacitors. *Electrochimica Acta* **209**, 486–497 (2016).
6. Seresht, R. J., Jahanshahi, M., Rashidi, A. & Ghoreyshi, A. A. Synthesize and characterization of graphene nanosheets with high surface area and nano-porous structure. *Applied Surface Science* **276**, 672–681 (2013).
7. Wu, X., Wang, Q., Zhang, W., Wang, Y. & Chen, W. Nano nickel oxide coated graphene/polyaniline composite film with high electrochemical performance for flexible supercapacitor. *Electrochimica Acta* **211**, 1066–1075 (2016).
8. Zhang, C., Lv, W., Tao, Y. & Yang, Q. H. Towards superior volumetric performance: design and preparation of novel carbon materials for energy storage. *Energy & Environmental Science* **8**, 1390–1403 (2015).
9. Simon, P. & Gogotsi, Y. Materials for electrochemical capacitors. *Nature Materials* **7**, 845–854 (2008).
10. Lv, Y. *et al.* A self-template synthesis of hierarchical porous carbon foams based on banana peel for supercapacitor electrodes. *Journal of Power Sources* **209**, 152–157 (2012).
11. Shang, T. X., Zhu, Y. M. & Jin, X. J. Preparation of Disused Composite Panels-Based Activated Carbon by Microwave Induced Activation for High Performance of Electric Double-Layer Capacitors: Microwave Power Effects. *Science of Advanced Materials* **8**, 1101–1107 (2016).
12. Chen, S., Zhu, J., Wu, X., Han, Q. & Wang, X. Graphene oxide–MnO₂ nanocomposites for supercapacitors. *Acs Nano* **4**, 2822–2830 (2010).
13. An, G. *et al.* Low-temperature synthesis of Mn(3)O(4) nanoparticles loaded on multi-walled carbon nanotubes and their application in electrochemical capacitors. *Nanotechnology* **19**, 1983–1989 (2008).
14. Chang, J. K., Hsu, S. H., Tsai, W. T. & Sun, I. W. A novel electrochemical process to prepare a high-porosity manganese oxide electrode with promising pseudocapacitive performance. *Journal of Power Sources* **177**, 676–680 (2008).
15. Beaudrouet, E., Salle, A. L. G. L. & Guyomard, D. Nanostructured manganese dioxides: Synthesis and properties as supercapacitor electrode materials. *Electrochimica Acta* **54**, 1240–1248 (2009).
16. Lei, Z., Shi, F. & Lu, L. Incorporation of MnO2-Coated Carbon Nanotubes between Graphene Sheets as Supercapacitor Electrode. *Acs Appl Mater Interfaces* **4**, 1058–1064 (2012).
17. Chen, W. *et al.* Hydrothermal synthesis of graphene-MnO₂ -polyaniline composite and its electrochemical performance. *Journal of Materials Science Materials in Electronics* **27**, 6816–6822 (2016).
18. Wu, P. *et al.* Synthesis and Characterization of Self-Standing and Highly Flexible δ-MnO₂@CNTs/CNTs Composite Films for Direct Use of Supercapacitor Electrodes. *Acs Applied Materials & Interfaces* **8**, 23721–23728 (2016).
19. Yu, G. *et al.* Solution-Processed Graphene/MnO₂ Nanostructured Textiles for High-Performance Electrochemical Capacitors. *Nano Letters* **11**, 2905–2911 (2011).
20. Yang, Q., Dong, L., Xu, C. & Kang, F. High-performance supercapacitors based on graphene/MnO₂/activated carbon fiber felt composite electrodes in different neutral electrolytes. *Rsc Advances* **6**, 12525–12529 (2016).
21. Xu, P. *et al.* Carbon Nanotube Fiber Based Stretchable Wire-Shaped Supercapacitors. *Advanced Energy Materials* **4**, 1300759 (2014).
22. Meng, Y. *et al.* All-Graphene Core-Sheath Microfibers for All-Solid-State, Stretchable Fibriform Supercapacitors and Wearable Electronic Textiles. *Advanced Materials* **25**, 2326–2331 (2013).
23. Kou, L. *et al.* Coaxial wet-spun yarn supercapacitors for high-energy density and safe wearable electronics. *Nature Communications* **5**, 3754–3754 (2014).
24. Chen, Q. *et al.* MnO₂ -modified hierarchical graphene fiber electrochemical supercapacitor. *Journal of Power Sources* **247**, 32–39 (2014).
25. Wu, Z. S. *et al.* High-energy MnO₂ nanowire/graphene and graphene asymmetric electrochemical capacitors. *ACS Nano* **4**, 5835–5842 (2010).
26. Yu, G. *et al.* Enhancing the Supercapacitor Performance of Graphene/MnO₂ Nanostructured Electrodes by Conductive Wrapping. *Nano Letters* **11**, 4438–4442 (2011).
27. Li, L., Raji, A. R. O. & Tour, J. M. Graphene-Wrapped MnO₂–Graphene Nanoribbons as Anode Materials for High-Performance Lithium Ion Batteries. *Advanced Materials* **25**, 6298–6302 (2013).
28. Gao, H., Xiao, F., Chi, B. C. & Duan, H. High-Performance Asymmetric Supercapacitor Based on Graphene Hydrogel and Nanostructured MnO₂. *Acs Applied Materials & Interfaces* **4**, 2801–2810 (2012).
29. Mu, B., Zhang, W. & Wang, A. Template synthesis of graphene/polyaniline hybrid hollow microspheres as electrode materials for high-performance supercapacitor. *Journal of Nanoparticle Research* **16**, 2432 (2014).

30. Iwashita, N., Chong, R. P., Fujimoto, H., Shiraishi, M. & Inagaki, M. Specification for a standard procedure of X-ray diffraction measurements on carbon materials. *Carbon* **42**, 701–714 (2004).
31. Chou, S., Wang, J. Z., Chew, S. Y., Liu, H. K. & Dou, S. X. Electrodeposition of MnO₂ nanowires on carbon nanotube paper as free-standing, flexible electrode for supercapacitors. *Electrochemistry Communications* **10**, 1724–1727 (2008).
32. Jin, X., Zhou, W., Zhang, S. & Chen, G. Z. Nanoscale microelectrochemical cells on carbon nanotubes. *Small* **3**, 1513–1517 (2007).
33. Zhang, J., Zhao, X., Huang, Z., Xu, T. & Zhang, Q. High-performance all-solid-state flexible supercapacitors based on manganese dioxide/carbon fibers. *Carbon* **107**, 844–851 (2016).
34. Ma, S. B., Ahn, K. Y., Lee, E. S., Oh, K. H. & Kim, K. B. Synthesis and characterization of manganese dioxide spontaneously coated on carbon nanotubes. *Carbon* **45**, 375–382 (2007).
35. Lu, X. *et al.* H-TiO₂@MnO₂//H-TiO₂@C Core–Shell Nanowires for High Performance and Flexible Asymmetric Supercapacitors. *Advanced Materials* **25**, 267–272 (2013).
36. Yan, J. *et al.* Carbonnanotube/MnO₂ composites synthesized by microwave-assisted method forsupercapacitors with high power and energy density. *Journal of Power Sources* **194**, 1202–1207 (2009).
37. Zhu, G. *et al.* Highly conductive three-dimensional MnO₂-carbon nanotube-graphene-Ni hybrid foam as a binder-free supercapacitor electrode. *Nanoscale* **6**, 1079–1085 (2014).
38. Mcdonough, J. R. *et al.* Carbon nanofiber supercapacitors with large areal capacitances. *Applied Physics Letters* **95**, 387–354 (2009).
39. Conway, B. E. *Electrochemical Supercapacitors.* (Plenum Press, 1999).
40. Zhai, T. *et al.* Oxygen vacancies enhancing capacitive properties of MnO₂ nanorods for wearable asymmetric supercapacitors. *Nano Energy* **8**, 255–263 (2014).
41. Pan, Z. *et al.* Ultra-endurance flexible all-solid-state asymmetric supercapacitors based on three-dimensionally coated MnO x nanosheets on nanoporous current collectors. *Nano Energy* **26**, 610–619 (2016).
42. Taberna, P. L., Simon, P. & Fauvarque, J. F. Electrochemical Characteristics and Impedance Spectroscopy Studies of Carbon-Carbon Supercapacitors. *Journal of the Electrochemical Society* **150**, A292–A300 (2003).
43. Yang, P. *et al.* Low-cost high-performance solid-state asymmetric supercapacitors based on MnO2 nanowires and Fe₂O₃ nanotubes. *Nano Letters* **14**, 731–736 (2014).
44. Lu, X. *et al.* Oxygen-deficient hematite nanorods as high-performance and novel negative electrodes for flexible asymmetric supercapacitors. *Advanced Materials* **26**, 3148–3155 (2014).
45. Zeng, Y. *et al.* Advanced Ti-Doped Fe2O3@PEDOT Core/Shell Anode for High-Energy Asymmetric Supercapacitors. *Advanced Energy Materials* **5**, 1402176 (2015).
46. Jr, W. S. H. & Offeman, R. E. Preparation of Graphitic Oxide. *Journal of the American Chemical Society* **80**, 1339–1339 (1958).
47. K., N. I. *et al.* Layer-by-Layer Assembly of Ultrathin Composite Films from Micron-Sized Graphite Oxide Sheets and Polycations. *Chemistry of Materials* **11**, 771–778 (1999).
48. Yu, H. R., Cho, S., Jung, M. J. & Lee, Y. S. Electrochemical and structural characteristics of activated carbon-based electrodes modified via phosphoric acid. *Microporous & Mesoporous Materials* **172**, 131–135 (2013).
49. Shang, T. X., Ren, R. Q., Zhu, Y. M. & Jin, X. J. Oxygen- and nitrogen-co-doped activated carbon from waste particleboard for potential application in high-performance capacitance. *Electrochimica Acta* **163**, 32–40 (2015).
50. Park, S. *et al.* Colloidal suspensions of highly reduced graphene oxide in a wide variety of organic solvents. *Nano Letters* **9**, 1593–1597 (2009).
51. Li, D., Müller, M. B., Gilje, S., Kaner, R. B. & Wallace, G. G. Processable aqueous dispersions of graphene nanosheets. *Nature Nanotechnology* **3**, 101–105 (2008).

Acknowledgements

Author Contributions

L.X., M.J. and X.J. designed the study. M.Y. and Y.L. contributed to the SEM, Raman, and XRD analysis. X.J. and F.Z. provided guidance for the whole study. L.X., and X.J. drew all the figures and wrote the main manuscript text. All authors approved the final manuscript.

Additional Information

Competing Interests: The authors declare that they have no competing interests.

Publisher's note: Springer Nature remains neutral with regard to jurisdictional claims in published maps and institutional affiliations.